Materials Today Sustainability 24 (2023) 100593

Contents lists available at ScienceDirect

Materials Today Sustainability

journal homepage: www.journals.elsevier.com/materials-today-sustainability

Sustainable β- and γ-cyclodextrins for development of highly permeable thin film composite nanofiltration membranes

Cristina Pina-Vidal [a,b], Jose Miguel Luque-Alled [a,b,*], Joaquín Coronas [a,b], Carlos Téllez [a,b,**]

[a] Instituto de Nanociencia y Materiales de Aragón (INMA) CSIC-Universidad de Zaragoza, 50018, Zaragoza, Spain
[b] Departamento de Ingeniería Química y Tecnologías Del Medio Ambiente, Universidad de Zaragoza, 50018, Zaragoza, Spain

ARTICLE INFO

Keywords:
Membrane
Nanofiltration
Thin film composite
Polyamide
Polyester
Cyclodextrins

ABSTRACT

The use of macromolecules, such as cyclodextrins (CDs), given their porosity and compatibility with organic materials, are very attractive for the progress of polymeric membranes in nanofiltration (NF) of aqueous dye solutions. Two types of membranes were fabricated. Firstly, β- and γ-CDs were incorporated to polyamide (PA) thin film composite (TFC) membranes. These membranes, named CD/MPD-TMC, were prepared by conventional interfacial polymerization —i.e., an aqueous solution of m-phenylenediamine (MPD) followed by a solution of trimesoyl chloride (TMC) in hexane— by replacing a certain amount of the MPD monomer with varying proportions of CDs. Secondly, two-step double-IP (TD-IP) membranes were fabricated as follows: CDs were deposited atop the polymer support, followed by addition of TMC —forming a polyester (PE) layer—, and subsequently the membrane surface was modified with MPD molecules. In both CD/MPD-TMC and TD-IP membranes, the presence of CDs improved the membrane performance, the latter configuration leading to much higher water permeances. The TD-IP membrane using β-CD achieved the highest water permeance of 10 L m^{-2} h^{-1}·bar^{-1} (LMH bar^{-1}) and a rejection of acridine orange dye (265 Da) greater than 98 %. This represents a 6-fold increase in water permeance compared to bare PA (1.6 LMH bar^{-1}). The enhanced water transport was mainly attributed to the more hydrophilic nature of the membranes and the presence of a PE layer with a porous structure and high pore connectivity. High dye rejection resulted from electrostatic and Donnan repulsions due to surface modification with MPD molecules.

1. Introduction

Production of fresh water has become a capital issue. World Economic Forum's Global Risks 2015 report highlighted water scarcity as the major problem for humanity in the coming years and underlined the necessity of overhauling techniques available for fresh-water generation [1]. Climate change has led to a decrease of the available natural water supplies, and consequently modern societies depend on their technology to produce fresh water from distinct water sources [2]. High energy-efficiency water generation systems are required to make the process economically affordable and environmentally sustainable. Thus, membrane technology emerges as an ideal alternative for several water treatment applications. Nanofiltration (NF) is a mature membrane-based technology successfully applied in numerous water treatment applications. This includes the removal of divalent and trivalent salts [3], as well as low molecular weight organic compounds, such as pharmaceutical products [4], pesticides [5], and organic dyes [6], from water. Most NF membranes are thin film composite (TFCs) membranes, which consists of an ultrathin selective layer, typically polyamide (PA), on top of a porous polymeric support. The main role of this polymeric support is to provide mechanical stability while offering low resistance towards transport of molecules. The ultrathin PA layer is prepared by an interfacial polymerization (IP) process. The formation of this layer occurs at the interface between two immiscible solvents, each

Abbreviations: NF, nanofiltration; TFC, thin film composite; TFN, thin film nanocomposite; PA, polyamide; PE, Polyester; AO, Acridine Orange; IP, interfacial polymerization; TMC, trimesoyl chloride; MPD, phenylenediamine; PI, polyimide; CD, cyclodextrin; WCA, water contact angle; SEM, scanning electron microscopy; TEM, transmission electron microscopy; AFM, atomic force microscopy; XPS, X-ray photoelectron spectroscopy; TD-IP, two-step double; R_a, average plane roughness; RMS, Root mean square; SD, standard deviation; Pd, palladium; NPs, nanoparticles; PEG, Polyethyleneglycol.

* Corresponding author. Instituto de Nanociencia y Materiales de Aragón (INMA) CSIC-Universidad de Zaragoza, 50018 Zaragoza, Spain.
** Corresponding author. Instituto de Nanociencia y Materiales de Aragón (INMA) CSIC-Universidad de Zaragoza, 50018 Zaragoza, Spain.
E-mail addresses: jose.luque@unizar.es (J.M. Luque-Alled), ctellez@unizar.es (C. Téllez).

https://doi.org/10.1016/j.mtsust.2023.100593
Received 19 June 2023; Received in revised form 22 September 2023; Accepted 16 October 2023
Available online 20 October 2023

containing one monomer. The diffusion of one monomer into the solution of the other monomer results in polymerization. As the polymer layer forms at the interface, it creates a dense layer that restricts the diffusion of monomers between solutions, thus inhibiting further growth. These IP reactions typically involve polycondensation reactions between a diamine monomer, typically m-phenylenediamine (MPD) or piperazine (PIP) dissolved in water, and trimesoyl chloride (TMC) monomer dissolved in hexane or toluene. The inverse order of addition of the phases in the preparation of PA has also been studied (i.e. organic phase first, then aqueous phase), being called inverse or reverse IP [7].

The addition of nanomaterials to TFC membranes to prepare what is known as thin film nanocomposite membranes is an active field of research. In fact, nanomaterials have a strong potential to improve the permeation properties of NF membranes. First Zeolite nanoparticles, and later metal-organic frameworks (MOFs), have gathered lots of attention due to their high porosity, well-defined pore size, controlled particle size, and high crystallinity [8,9]. 2D materials, e.g. graphene and its derivatives [10] or boron nitride [11], are of particular interest as they exhibit extremely high surface areas derived from their ultrathin nature. Porous organic macromolecules have rapidly emerged as promising candidates to constitute TFC membranes since they combine the attractive features of porous nanoparticles with characteristics of organic matter such as polymers, favoring their dispersibility and compatibility. Amongst these macromolecules, cyclodextrins (CD), cyclic oligosaccharides, have been widely studied due to their unique 3D hollow bowl structure, high porosity, well-defined pore size, high crystallinity, and wide range of available options with distinct inner cavity sizes [12].

β-CD, with an empirical formula of $C_{42}H_{70}O_{35}$, is made of seven molecules of glucose giving rise to a cavity diameter of up to 0.78 nm. It is the preferred choice for membrane applications since it is the most available and cost-effective option and possesses a hydrophobic inner cavity and numerous hydroxyl groups in the external surface (see Fig. 1a). These hydroxyl functional groups have the potential to improve the compatibility with the polymer chains and are also used for particle functionalization or for polymerization reactions [13–15]. Several studies report IP reactions between β-CD and acyl chloride monomers (typically TMC). These reactions occur after deprotonation of the hydroxyl groups in β-CD resulting in the fabrication of TFC membranes containing macromolecules [16,17]. γ-CD (empirical formula $C_{48}H_{80}O_{40}$) is made of eight molecules of glucose. While it shares many of the attractive features of β-CD, such as hydrophilicity, compatibility with polymers, and hydroxyl functional groups, γ-CD has a larger inner cavity diameter (0.95 nm, Fig. 1b) as compared to β-CD (0.78 nm, Fig. 1a). γ-CD has also been involved in the preparation of TFC and CD/MPD-TMC membranes [12,18], even though is not as popular as β-CD.

In this work, to improve the NF performance of PA TFC membranes, β- and γ-CD macromolecules were incorporated using two different strategies (Fig. 2): i) preparation of CD/MPD-TMC membranes with different CD loadings, and ii) a two-step process where CDs were first deposited over the P84® support, reacted with TMC forming a polyester (PE) layer, and then the remaining functional groups on the surface were reacted with MPD resulting in what latter is called as "two-step double-IP (TD-IP) membranes". The formation of these hybrid structures using two IP reactions at independent steps is new in the literature, while the use of non-functionalized cyclodextrin and polyimide support for aqueous separations is also scarce. Membrane characterization by water contact angle (WCA), scanning electron microscopy (SEM), transmission electron microscopy (TEM), atomic force microscopy (AFM), fourier transform infrared spectroscopy (FTIR), X-ray diffraction (XRD), and X-ray photoelectron spectroscopy (XPS) were employed to reveal the morphology, wetting properties, and chemistry of pure TFCs, CD/MPD-TMC and TD-IP membranes. The prepared membranes were evaluated for NF of aqueous solutions containing acridine orange (AO) small dye (265 Da).

2. Materials and methods

2.1. Materials

The following reagents were used for membrane preparation. β-cyclodextrin (β-CD) and γ-cyclodextrin (γ-CD) were supplied by Sigma-Aldrich. Other chemicals used for IP reaction, such as m-phenylenediamine (MPD, 99 %) and trimesoyl chloride (TMC, 98 %) were also supplied by Sigma Aldrich. n-Hexane (extra pure) was purchased from Scharlab. For the support preparation, polyimide P84® was purchased from HP polymer GmbH, dimethyl sulfoxide (DMSO, 99.8 %) was supplied by Carlo Erba, isopropyl alcohol (for HPLC, 99.9 %) was supplied from Honeywell, and polyethylene glycol (PEG 400) was obtained from Scharlab. In order to provide mechanical stability to the supports, a polypropylene non-woven (PP) was used as backing material supplied by Freudenberg Performance Materials. The rejection tests were evaluated using Acridine Orange (AO, 55 % of purity) as organic dye provided by Acros Organics, and Polyethylene Glycol (PEG) of different molecular weights (200, 400, 600, and 1500 Da) were acquired from Sigma Aldrich.

2.2. Preparation of PI supports

The polyimide P84® supports were prepared following a previous report [21]. A dope solution of 24 % (w/w) was prepared by dissolving

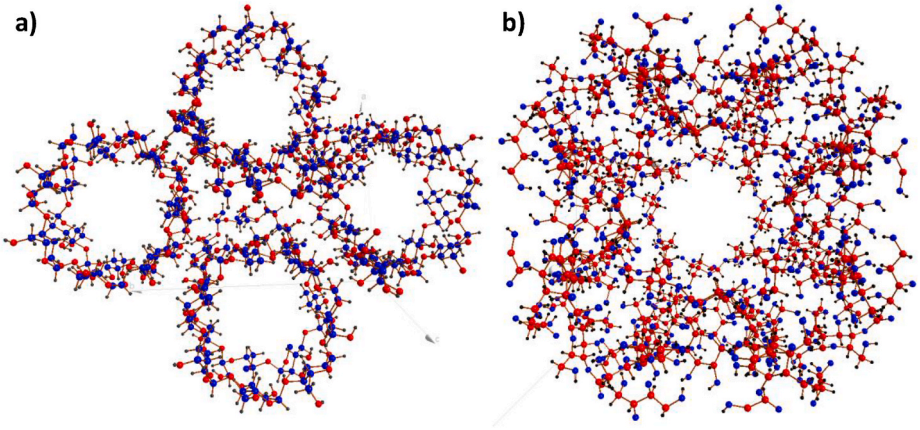

Fig. 1. β-cyclodextrin (a) and γ-cyclodextrin (b) structures showing porosity, with C, O and H atoms in blue, red and black respectively. These structures were built with Diamond 3.2 from the corresponding CIF files [19,20].

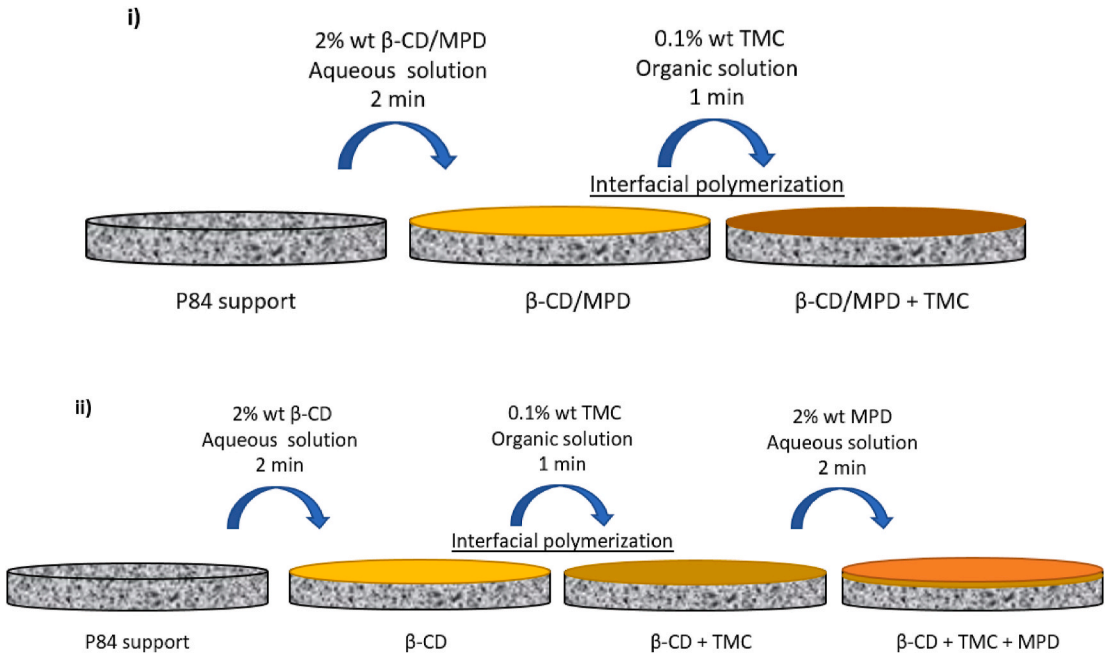

Fig. 2. Schematic diagram of membrane preparation of conventional one-step CD/MPD-TMC membranes (a) and two-step double-IP (TD-IP) membranes (b).

P84® in DMSO and stirring overnight. Once dissolved, the solution was allowed to stand until the air bubbles disappeared. Then, the solution was cast on a polypropylene non-woven backing material at a casting speed of 0.04 m s^{-1} using a casting knife (Elcometer 4340 automatic film applicator) set at a thickness of 250 μm. Immediately after casting, the membrane was immersed in a deionized water bath at ambient temperature, where the phase inversion occurred. After 10 min, the membrane supports were transferred to a freshwater bath and left for 1 h. The wet supports were then immersed into two consecutive baths of isopropyl alcohol, each for a duration of 1 h, to remove any remaining water or DMSO. Finally, the supports were submerged in a solution composed of a 3:2 vol ratio of polyethylene glycol (PEG) to isopropyl alcohol and were left overnight to allow the pores to be impregnated with the PEG. Then, the supports were dried with tissue paper and stored for later use.

2.3. Preparation of membranes

As shown in Fig. 2, two different types of PE/PA membranes were prepared, named CD/MPD-TMC and TD-IP membranes.

For the preparation of CD/MPD-TMC membranes, two solutions were employed: i) an aqueous solution of 2 % (w·v^{-1}) of total monomer concentration (including both CDs and MPD) with varying CD/MPD ratios (0/100, 20/80, 50/50 and 100/0), and ii) an organic solution of 0.1 % (w·v^{-1}) TMC in n-hexane. Once dissolved, a 16 cm^2 support disk was placed in a glass filtration holder. For the interfacial polymerization reaction, 30 mL of the aqueous solution was poured over the support and left for 2 min. After this time, the excess of the aqueous solution was removed, and the membrane was drained using a rubber brayer roller. Then, 30 mL of TMC solution was added and left for 1 min. After that, the excess organic solution was poured away, and 10 mL of n-hexane was added twice to stop the reaction and to remove the unreacted TMC. Table 1 shows the CD/MPD-TMC membranes fabricated with different ratios of β-CD or γ-CD and MPD, while the concentration of TMC is fixed at 0.1 % (w·v^{-1}). When the CD/MPD ratio was 0/100 a conventional PA TFC membrane was formed, whereas when the CD/MPD ratio was 100/0 a CD-based PE TFC was produced.

For the preparation of TD-IP membranes, a PE layer was first formed, followed by reaction with MPD monomers. To begin with, an aqueous solution of 2 % (w·v^{-1}) of CD was poured over the PI support. After 2 min, the solution was taken away and a rubber brayer roller was employed to remove remaining drops on the support surface. An organic solution of 0.1 % (w·v^{-1}) TMC was then added and left for 1 min to allow reaction with CDs and the formation of the PE. The organic solution was drained, and the support was left to dry inside of the fume cupboard at room temperature for 5 min (time at which it is assumed that all the n-hexane was evaporated from the membrane surface). Afterwards, an aqueous solution of 2 % (w·v^{-1}) MPD was poured over the membrane and removed after 2 min when reaction with TMC molecules is believed to be completed [21,22]. These membranes are referred in Table 1 as

Table 1
Sum up of all membranes used in this work including details such as the preparation procedure, CD/MPD ratio used in the aqueous phase, and type of CD.

Membrane code	Preparation procedure	CD/MPD ratio in aqueous phase	Type of CD
PA[a]	Conventional IP[b]	0/100	–
CD/MPD-TMC_20β	Conventional IP[b]	20/80	β
CD/MPD-TMC_50β	Conventional IP[b]	50/50	β
PE_β[c]	Conventional IP[b]	100/0	β
CD/MPD-TMC_20γ	Conventional IP[b]	20/80	γ
CD/MPD-TMC_50γ	Conventional IP[b]	50/50	γ
PE_γ[c]	Conventional IP[b]	100/0	γ
TD-IP_β	β-CD deposition/ inverse IP	1st step: 100/0[d] 2nd step: 0/100[e]	β
TD-IP_γ	γ-CD deposition/ inverse IP	1st step: 100/0[d] 2nd step: 0/100[e]	γ

[a] PA corresponds to a conventional TFC membrane made of MPD and TMC.
[b] Total monomer concentration of 2 % (w·v^{-1}) in the aqueous solution. For instance, CD/MPD ratio of 20/80, then 0.4 % of CD and 1.6 % of MPD in the aqueous solution.
[c] PE refers to a TFC membrane made of CDs and TMC.
[d] 1st step involves using a 2 % (w·v^{-1}) CDs aqueous solution for CD deposition.
[e] 2nd step involves using a 2 % (w·v^{-1}) MPD aqueous solution for the inversed IP reaction.

TD-IP_β and TD-IP_γ where TD accounts for "two-step double", and β or γ for the type of CD used.

Right after membrane fabrication, all prepared membranes were introduced in an oven at 60 °C for 15 min to ensure cross-linking of the prepared selective layers. Finally, the membranes were stored in DI water in the fridge (4 °C) for testing within 48 h of preparation.

2.4. Characterization techniques

Surface and cross-sectional images of the membranes were observed by scanning electron microscopy (SEM) using an Inspect-F-50 microscope (FEI) operated at 10 kV. Cross-sectional specimen samples were prepared by freeze-fracturing inside liquid N_2. All samples were mounted on metal holders and coated with palladium under vacuum conditions to provide electrical conductivity.

Selective ultrathin cross-sectional membrane specimens were obtained by ultramicrotomy and imaged using a FEI Tecnai T20 microscope operated at 200 kV of accelerating voltage to investigate the membrane structure. An ultramicrotomy process was carried out to obtain ultrathin sections of 70 nm. First, the membranes samples undergo two different treatments: i) deposition of a thin layer (ca. 5 nm thick) of palladium (Pd) nanoparticles (NPs), and ii) immersion in an OsO_4 solution (2 wt% in H_2O) for 2 h at room temperature. Subsequently, the samples treated with OsO_4 were dehydrated using ethanolic solutions. Both Pd coated and OsO_4 treated samples were embedded in EMBed 812 resin with the aid of a vacuum overnight. The resin was allowed to polymerize for 3 days at 60 °C. The cutting process was performed at room temperature using a diamond knife on a Leica EM UC7 ultramicrotome device at an angle of 6°, at a step-size of 70 nm, and at a speed of 1 mm s^{-1}. The ultrathin sections were fished with a carbon 300 mesh copper grids and left to dry for 24 h prior to imaging.

Quantitative surface roughness analysis of the membranes was carried out using an atomic force microscopy (AFM) at a resonant frequency of 300 kHz with a force constant of 40 mN and a silicon cantilever provided by Bruker. The AFM device was a Veeco MultiMode 8 scanning probe microscope in tapping mode. From these measurements, the average plane roughness (R_a) and the root mean square (RMS) parameters were determined. The scan size of each sample was 10 μm × 10 μm.

The hydrophobic/hydrophilic nature of the membrane was determined using a contact angle goniometer (Krüss DSA 10 MK2)) at 25 °C. Three different specimens for each membrane were characterized to obtain water contact angle (WCA) average values with their corresponding standard deviation (SD).

Powder X-ray diffraction (XRD) was performed at room temperature in an Empyrean PANalytical diffractometer with a Cu-K_α radiation source (λ = 1.5406 Å). Data were collected in the 2θ range from 2.5° to 40° at a scanning rate of 0.01°•s^{-1}.

Attenuated Total Reflection Fourier Transform Infrared Spectroscopy (ATR-FTIR) was used to identify functional groups on the surface of the membrane. The spectra were recorded in the 600-2000 cm^{-1} wavenumber range with an accuracy of 4 cm^{-1}, using a Bruker Vertex 70 FTIR spectrometer equipped with a deuterated triglycine sulphate detector and a Golden Gate diamond ATR accessory.

The chemical structures of the TD-IP membranes were determined by XPS using an AXIS Ultra DLD system from Kratos Analytical with a monochromated Al Kα source (1486.6 eV) at 15 kV, 10 mA, and a power of 150 W. XPS spectra were analyzed using a CasaXPS software.

2.5. Nanofiltration experiments

Nanofiltration experiments were carried out at 20 bar of feed pressure under stirring at room temperature (25 °C) in a dead-end membrane module (Sterlitech HP4750). The membrane performance was evaluated using 250 mL of feed solution with an acridine orange (AO) concentration in DI water of 20 mg•L^{-1}. The flat membrane effective area was 2.27 cm^2. All membranes were stabilized under 20 bar for 1 h before testing. The permeance and the rejection were calculated using the following equations:

$$Permeance = \frac{V}{\Delta P \times A \times t} \quad (1)$$

$$Rejection\ (\%) = \left(1 - \frac{C_{permeate}}{C_{residue}}\right) \times 100 \quad (2)$$

where, V is the volume of collected permeate (L), ΔP is the pressure difference (bar) used in experiments between the residue and permeate, A is the effective area of the membrane (m^2), t is the time for permeate collection (h). Both concentrations, permeate ($C_{permeate}$) and residue ($C_{residue}$), were measured by an UV spectrometer (Jasco V-670 spectrophotometer) using water as solvent at a fixed wavelength of 490 nm for AO.

Molecular Weight Cut-Off (MWCO) experiments were conducted using independent PEG solutions in water with varying molecular weights (200, 400, 600, and 1500 Da), each at a concentration of 5 g•L^{-1}. Quantification of PEG was carried out using high performance liquid chromatography (HPLC) equipped with an in-line degasser AF (Waters), a dual-piston pump (Waters 1515 isocratic HPLC pump) and a refractive index detector (Waters 2414). 5 μl of sample solutions were injected for each analysis. Sample solutions were analyzed using water as a mobile phase, a flowrate of 1.0 ml•min^{-1} and a temperature of 30 °C.

3. Results and discussion

3.1. Membranes characterization

Fig. 3 shows top-view SEM images of the prepared membranes. In Fig. 3a, corresponding to a pure PA membrane, the expected nodular and ridge-and-valley morphologies are clearly visible [10]. In the case of β- and γ-CD/MPD-TMC membranes with a CD/MPD ratio of 50:50 (Fig. 3b and c, respectively), the membrane surface seems very similar to that of pure PA membranes. Fig. 3d and e reveal the surface of TD-IP membranes (TD-IP_β and TD-IP_γ, respectively) where an unusual morphology, consisting of a number of round-shaped cavities, is observed. This sort of structure has been previously reported when forming polyarylate layers that were synthesized using CDs and TMC monomers [23]. Amongst TD-IP membranes, those with β-CD (Fig. 3d) show more prominent features as compared to those having γ-CDs (Fig. 3e). This suggests that the PE layer containing the CDs governs the morphology of the final membrane. During the formation of the PE layer polycondensation reactions between the hydroxyl groups in CDs (both β- and γ-) and the acyl chloride groups in TMC molecules take place (as will be proven by XPS). Later, MPD reacts with unreacted groups in TMC molecules in the PE layer. Owing to the organic nature of all the membrane components, which exhibit similar contrast under SEM, it is not possible to distinguish the presence of CD in any of the SEM images.

Static WCA was used to study the wetting properties of the membranes (Fig. 4). A value of 60° was found for the pure PA layer, similar to that reported by other authors [18]. The addition of both β- and γ-CD decreased the WCA of the membrane, e.g. CD-TMC_20β and CD-TMC_20γ vs. PA. As the concentration of CD increased, the WCA of CD/MPD-TMC membranes dropped with the lowest WCA values for PE_β and PE_γ. This can be attributed to the strong hydrophilicity of the external surface of the CDs with a high concentration of hydroxyl groups [18,24]. TD-IP membranes are essentially PE (β- or γ-) membranes that have been modified with MPD molecules. This configuration showed higher WCA values as compared to their counterparts (PE_ β and PE_γ). However, as compared to control pure PA membranes, TD-IP membranes (both β- and γ-) have lower WCA, which can be attributed to both external hydrophilicity of the CD and presence of several pores with high

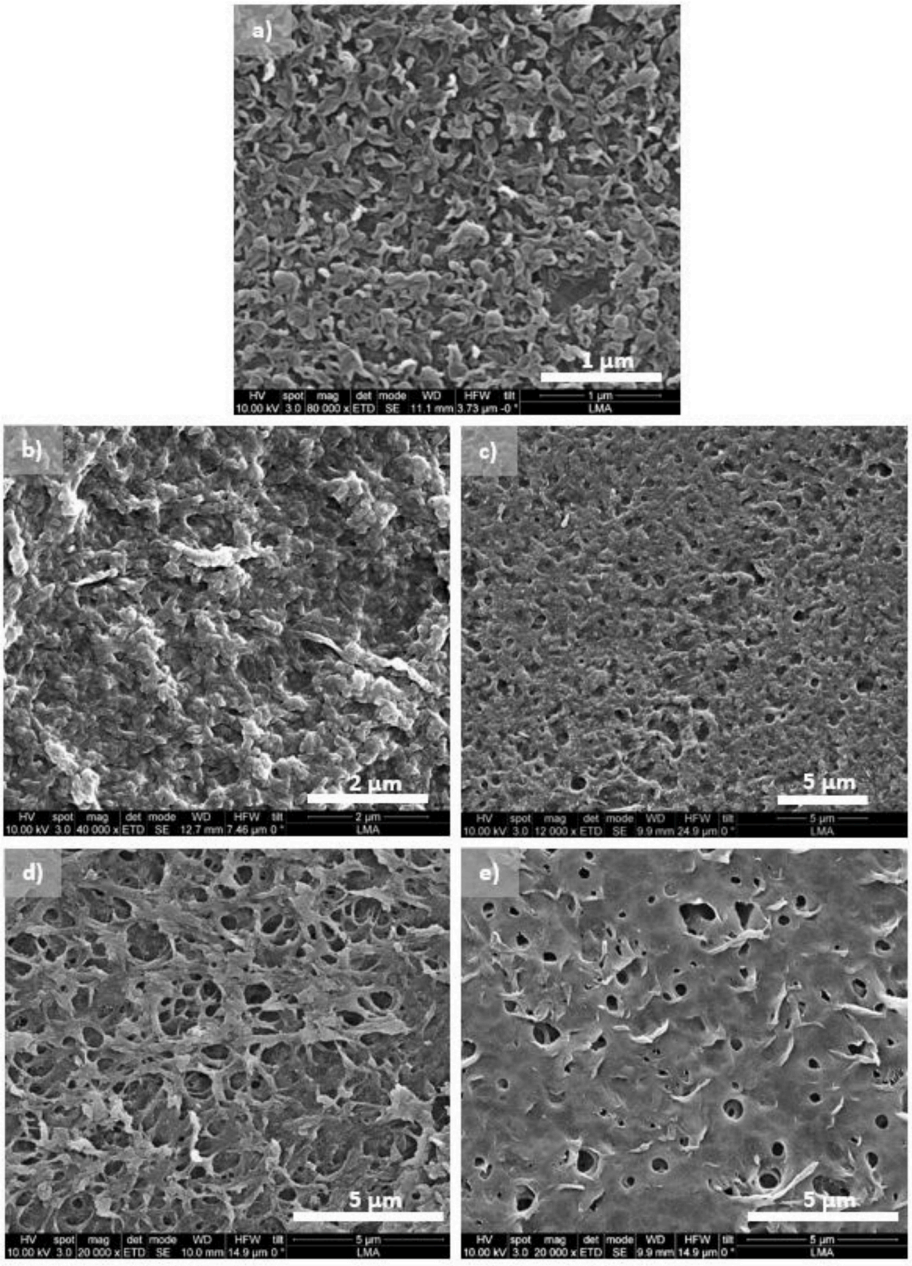

Fig. 3. Surface SEM micrographs of PA membrane (a), CD/MPD-TMC_50β (b), CD/MPD-TMC_50γ (c), TD-IP_ β (d), and TD-IP_γ (e).

water sorption capacity. Amongst both types of CDs, the WCA values are, within the experimental error, very similar for membranes with equivalent loading of CDs, e.g. CD-TMC_20β and CD-TMC_20γ. The chemical composition of both CDs is analogous, and their pores should not have such a significant impact on the surface properties after the formation of the PE film, which explains their similar WCA behavior.

XPS was employed to study the formation of the polymer structures by assessing how the atomic compositions evolved and which bonds were formed during all the steps of the TD-IP membrane fabrication. The following samples were analyzed: i) bare P84® support, ii) P84®-CD, which refers to the P84® support coated with β-CDs, iii) P84®-CD-TMC, which is produced by addition of TMC to P84®-CD and corresponds to a PE_β membrane, and iv) P84®-CD-TMC-MPD, formed by adding MPD to P84®-CD-TMC, known as a TD-IP_β membrane. Fig. 5 shows the high resolution C 1s spectra of all the samples tested. Fig. 5a, corresponding to P84®, shows three main peaks attributed to C–C/C=C at 284.5 eV, C–N at 285.5 eV, and C=O (including N–C=O and Ar–C=O bonds) at 287.9 eV, as well as a satellite peak arising from the presence of aromatic structures, i.e. π-π* [25,26]. The deposition of β-CD on top of P84® is depicted in the spectrum corresponding to P84®-βCD (Fig. 5b) as a new peak at 286.2 eV that arises from the presence of abundant C–O bonds in β-CD [27,28]. However, that peak appears to vanish in the P84®-βCD-TMC spectrum (Fig. 5c) because ester functional groups (C=O peak at 287.7 eV) are formed due to the nucleophilic substitution reactions between hydroxyl groups in β-CD and acyl chloride groups in TMC. The formation of a PE layer is promoted at basic pH, while the β-CD solution used in this study has a pH of ~7–8. Hence, some acyl-chloride groups are likely to remain unreacted, and they can participate in additional reactions with stronger nucleophiles, such as amine groups in MPD molecules [29]. The high resolution C 1s spectrum of P84®-βCD-TMC-MPD (Fig. 5d) is very similar to that of P84®-βCD-TMC since MPD molecules also contain C=C and C–N bonds, and the formation of the polyamide (i.e. N–C=O) contributes to the C=O peak.

The atomic percentages together with their corresponding C/N and

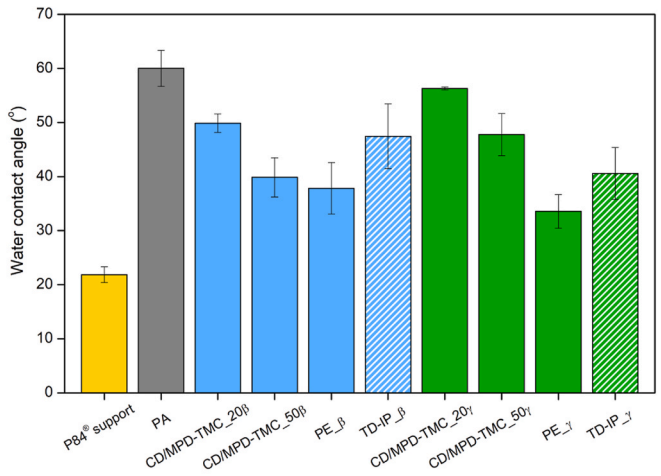

Fig. 4. WCA of all prepared membranes along with their corresponding standard deviation.

C/O ratios for all samples are shown in Table 2. The deposition of β-CDs ($C_{42}H_{70}O_{35}$) having abundant hydroxyl groups results in a decrease of the C/O ratio, i.e. values of 4.3 and 3.6 for P84® and P84®-βCD, respectively. In P84®-βCD-TMC, the addition of TMC ($C_6H_3(COCl)_3$) and its reaction with CDs leads to a slight rise in the C/N (value of 17.0) in comparison with that of P84®-βCD (with a value of 16.3). A significant increase in C/O ratio is observed for P84®-βCD-TMC-MPD (value of 5.9) as compared to P84®-βCD-TMC (value of 3.6), which can be attributed to the incorporation of carbon atoms coming from MPD molecules ($C_6H_4(NH_2)_2$). This suggests that MPD molecules react with unreacted acyl chloride functional groups in P84®-βCD-TMC. In addition, after incorporation of MPD, a lower C/N ratio of 15 is found (compared to 17 for P84®-βCD-TMC) due to the abundance of nitrogen atoms in the amine monomer MPD.

To study the topography of the membrane surface, AFM measurements were conducted, and the corresponding 2D and 3D images together with their R_a and RMS parameters are shown in Fig. 6. The pure PA membrane exhibited RMS and R_a values of 81 nm and 62 nm, respectively, which were similar than typical values reported for PA in bibliography [18]. Compared to this membrane, the TD-IP_β membrane exhibited a smoother surface with RMS and R_a values of 42 nm and 30 nm, respectively, likely due to the formation of a β-CD-based PE layer that results in flatter membranes than pure PA TFC membranes [30,31]. The roughness of CD/MPD-TMC_50β and CD/MPD-TMC_50γ

Table 2
C/N and C/O ratios of membranes obtained by XPS analysis.

Sample	at.% C	at.% N	at.% O	C/N ratio	C/O ratio
P84®	77.3	5.6	18.1	13.8	4.3
P84®-βCD	74.8	4.6	20.6	16.3	3.6
P84®-βCD-TMC (CD-TMC_100β)	74.9	4.4	20.7	17.0	3.6
P84®-βCD-TMC-MPD (TD-IP_β)	80.9	5.4	13.8	15.0	5.9

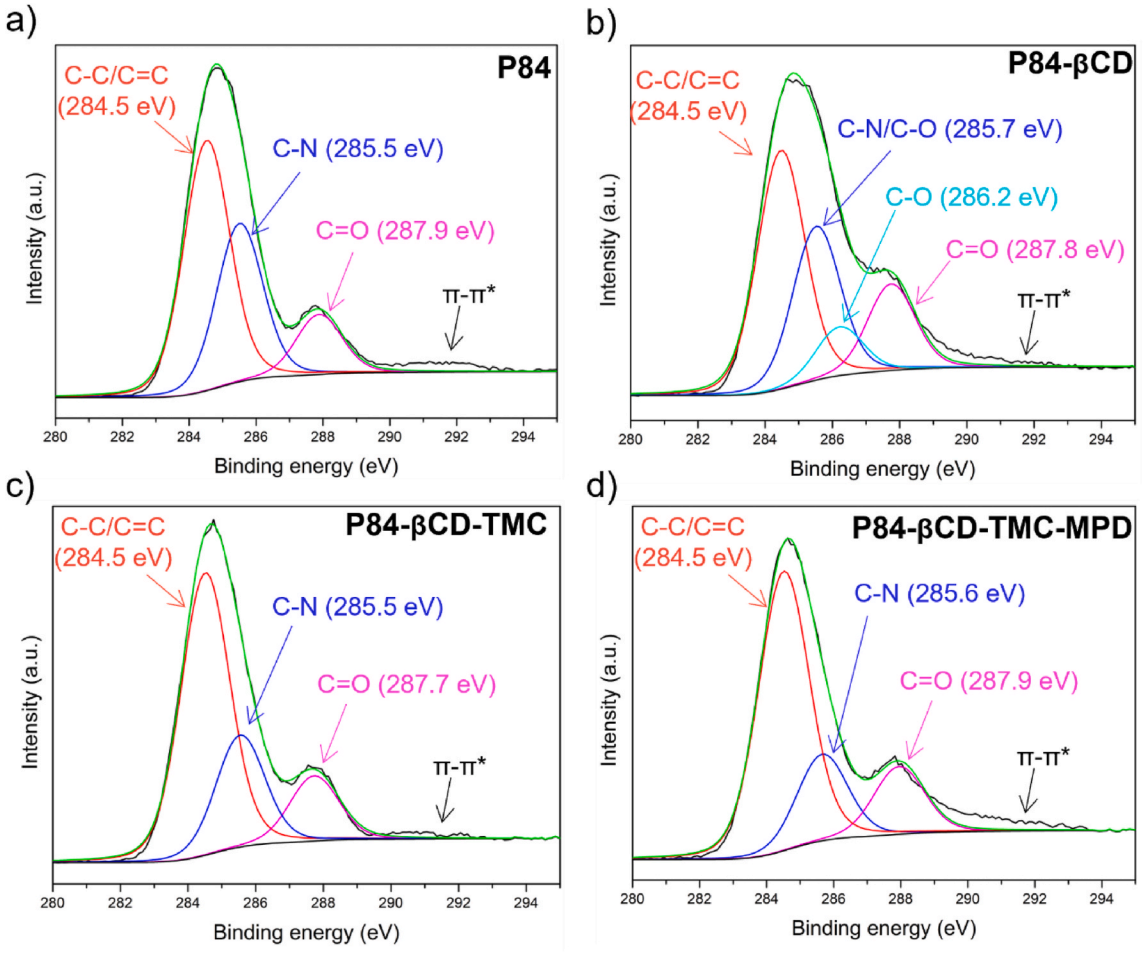

Fig. 5. XPS high resolution C 1s spectra of P84® support (a), and membranes P84®-βCD (b), P84®-βCD-TMC (c), and P84®-βCD-TMC-MPD (d).

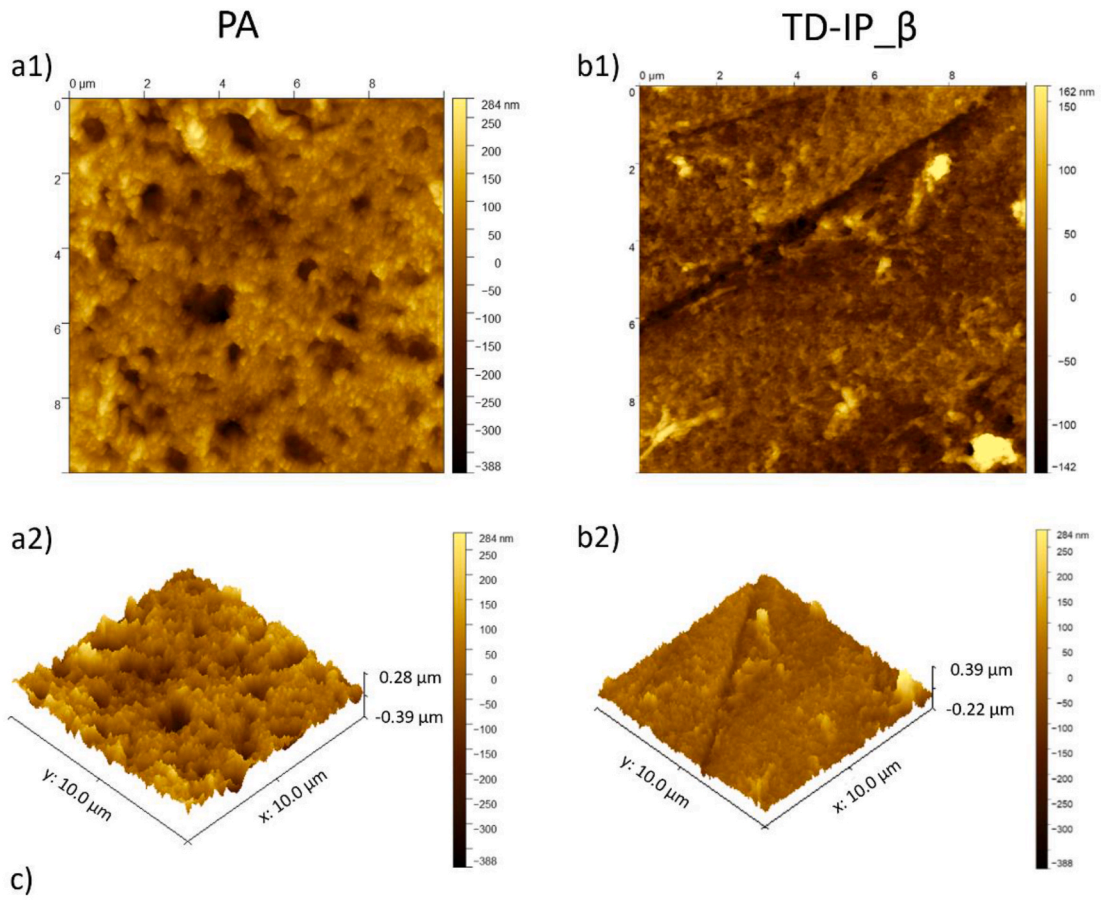

Membrane code	Average plane roughness (R_a, nm)	Root mean square (RMS, nm)
PA	62	81
CD/MPD-TMC_50β	35	45
CD/MPD-TMC_50γ	40	51
TD-IP_β	30	42

Fig. 6. AFM images of PA membrane (a1 and a2) and TD-IP_β membrane (b1 and b2) and sum up of the roughness parameters for PA, CD/MPD-TMC_50β, CD/MPD-TMC_50γ and TD-IP_ β membranes. a1) and b1) have different scale bar on the z-axis in order to clearly see the voids in the membrane surface. a2) and b2) images have the same scale bar on the z-axis to see the lower roughness of TD-IP_ β membrane.

membranes was also analyzed by AFM (images shown in Figure S1). Their roughness parameters are included in Fig. 6c for comparison with pure PA TFCs and TD-IP membranes. The incorporation of CDs reduces the surface roughness as compared to pure PA TFC membranes. This finding confirms our previous observation, i.e. the PE formation is characteristically smoother than that of PA layer.

Figures S2 and S3 show the ATR-FTIR analysis of the prepared membranes together with the spectra of pure β/γ-CDs. Despite the presence of peaks corresponding to both CDs are observed in the spectra of CD/MPD-TMC and TD-IP membranes, it should be noted that P84® also exhibits peaks at the same wavenumbers [32,33]. Due to the similar chemical nature of P84®, PE and PA, little information can be inferred. The main peaks of P84® (at 720, 1380, and 1713 cm^{-1}) exhibit reduced intensity compared to PA, CD/MPD-TMC, PE, and TD-IP membranes. Though the peak at 1080 cm^{-1} maintains a similar intensity for all membranes, the shape of this peak in P84® notably differs from the other membranes. This suggests the formation of a PE, a PA, or a combination of both on top of the P84® support. Yet, differentiating between PE and PA is challenging, given their inherent similarities. The PE and PA layers are much thinner as compared to the P84® support. Consequently, the peaks from the P84® support dominate the ATR-FTIR spectra of the membranes, resulting in a very diminished signal from the PE or PA layers.

The X-ray diffraction (XRD) patterns of selected membranes are shown in Figure S4. The pattern of PA membrane is very similar to that of the TD-IP membranes and peaks corresponding to CD cannot be identified. Even if CDs are crystalline materials, the lack of their peaks in the XRD patterns is in line with the SEM observation suggesting that the CD was evenly distributed without forming particles that could be detected by this technique. In addition, the amorphous nature of the P84® leads to a prominent background signal which hinders obtaining useful information.

Fig. 7 presents TEM images of PA TFC (a, b, and c) and TD-IP_β membranes (d). Two different TEM specimen treatments were

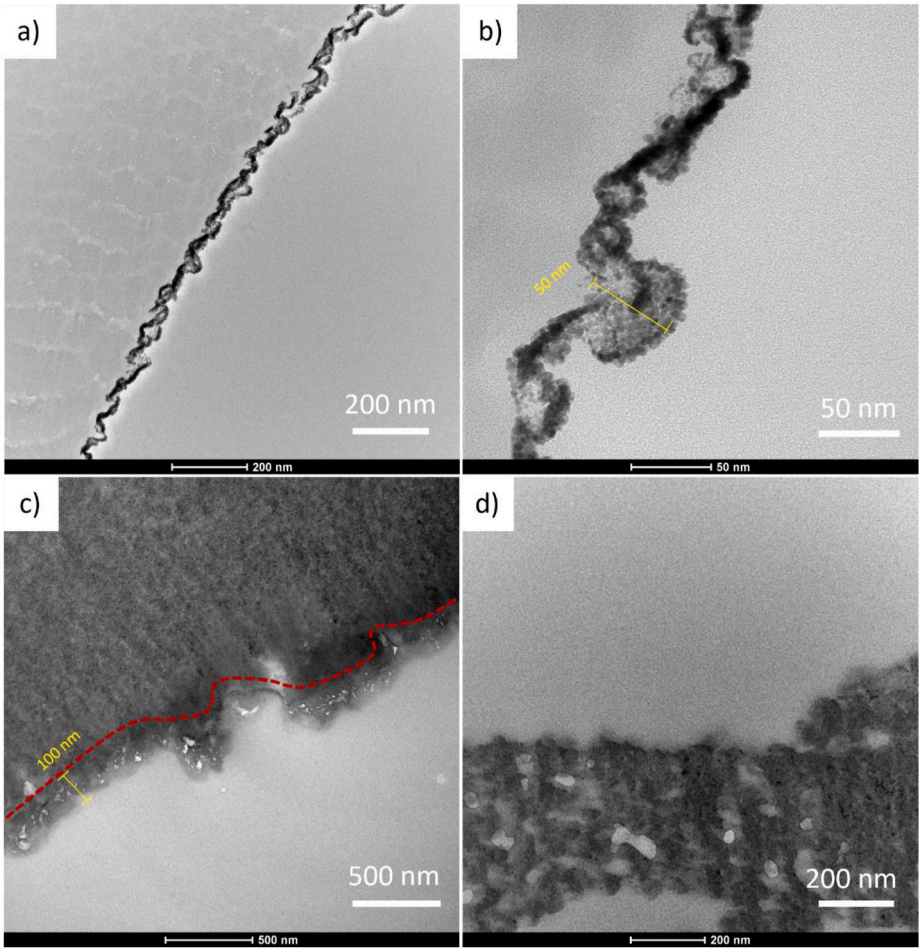

Fig. 7. Cross-sectional TEM images of PA TFC membranes over P84® (a, b, and c), and TD-IP_β (d). Panels a–b correspond to PA TFC membranes that have been coated with a thin layer of Pd NPs (ca. 5 nm). Panels c–d correspond to pure PA TFC and TD-IP_β membranes, respectively, treated with OsO_4 solution.

conducted to help identify the PA layer: i) coating with Pd NPs, and ii) immersion in an OsO_4 solution. After depositing Pd NPs onto the PA surface (Fig. 7a and b), the contrast is greatly enhanced, allowing for clear differentiation of the profile of the PA layer. In addition, this also enables the measurement of the height of the protuberances, approximately 50 nm. After treating the samples with OsO_4, enhanced contrast is observed for both the P84® support layer and the PA layer. OsO_4 reacts with carbon-carbon double bonds in the polymer structure, intensifying the contrast under TEM for both PI and PA containing these functional groups. Thus, the PA layer can be distinctly identified, and the presence of nodules within this layer are clearly visible (Fig. 7c). While a thickness of approximately 100 nm is identified, this measurement includes the nodules, which are filled with empty space. Consequently, the actual thickness is probably much lower. On the contrary, Fig. 7d, corresponding to TD-IP_β membranes treated with OsO_4, reveals no distinguishable thin layer. Instead, a polymer layer with discrete pores directly beneath the surface is identified atop the P84® support. This morphology agrees with that shown in the SEM images (Fig. 3d), i.e. existence of abundant shallow cavities near the surface. To understand the structure of TD-IP_β membranes, it is required to examine the membrane formation process. As a result, the following mechanism is proposed: i) P84® supports are coated with CDs, ii) when the n-hexane solution containing TMC is added, hydrophilic CDs have a tendency to agglomerate with the aim of reducing their contact area with the nonpolar organic solution, iii) as TMC molecules encounter CDs, attractive electronic interactions and polycondensation reactions take place between them leading to the formation of a PE layer, and iv) when an aqueous solution of MPD is added, the amine molecules react with unreacted acyl chloride groups in the TMC molecules.

3.2. Membranes performance

The small dye AO (265 Da) was chosen to assess the NF performance of the membranes prepared. The water permeance and AO dye rejection of the prepared membranes is shown in Fig. 8. Pure PA membranes showed a water permeance of 1.6 ± 0.7 $L \bullet m^{-2} \bullet h^{-1} \cdot bar^{-1}$ ($LMHbar^{-1}$) and a AO dye rejection of 99.2 %, similar to that found by other authors [34]. The formation of CD/MPD-TMC membranes improved the membrane water permeance due to the hydrophilicity and porous structure of the macromolecules [17]. Both β- and γ-CDs are often referred as hydrophilic materials due to the abundant hydroxyl functional groups in their external surface, but their inner cavities exhibit hydrophobic properties that account for the existence of low-friction inter-connected channels through which water molecules easily pass [35]. CD/MPD-TMC membranes prepared with γ-CD led to higher water permeance than those prepared with β-CD, which can be attributed to the larger inner diameter of the γ phase (0.78 nm for β-CD and 0.95 nm for γ-CD [36]) and therefore lower hindrance towards water transport. When using γ-CDs and a CD/MPD ratio of 20/80, i.e. CD/MPD-TMC_20γ, a water permeance of 3.2 ± 0.1 LMH•bar-^{1} was achieved. This is the highest value among all CD/MPD-TMC membranes obtained in this work, and it is twice as high as that of the control PA membrane. The rejection of both CD/MPD-TMCs and the control PA membrane remain always at very high values (>99 %).

When a CD/MPD ratio of 100/0 is used, PE_β and PE_γ membranes are fabricated due to polycondensation reactions between hydroxyl

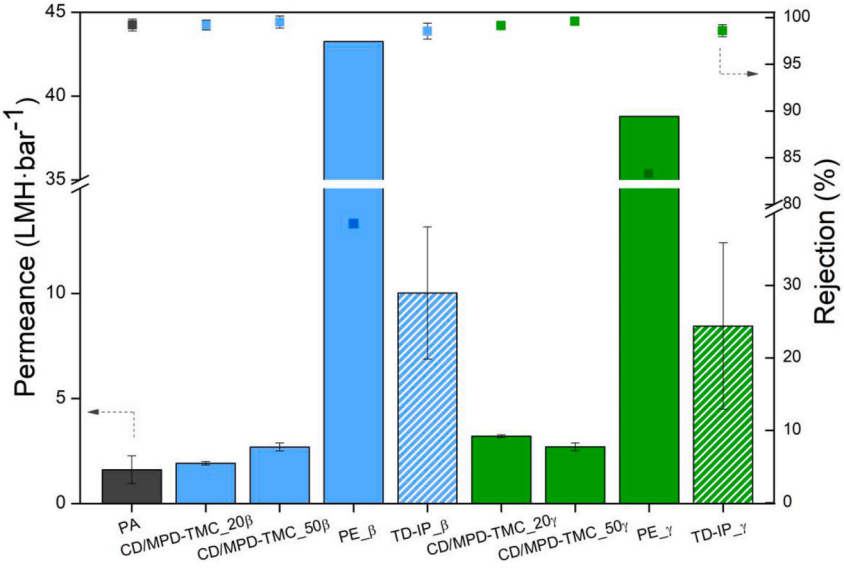

Fig. 8. Water NF performance of PA membrane, CD/MPD-TMC membranes (β- and γ-CD), PE_β and PE_γ membranes, and two-step membranes (TD-IP_β and TD-IP_γ). Water permeance and rejection values are collected in Table S1.

groups in CDs and acyl chloride groups in TMC molecules. Under the current conditions of synthesis (neutral pH and room temperature), IP reactions between CD and TMC are not much favored; deprotonation of hydroxyl groups present in CDs is required at high pH to accelerate polycondensation reactions. Then, the synthesized PE_β and PE_γ layers show remarkably high water permeance but unsatisfactory rejection of AO dye (<85 %). This is attributed to incomplete cross-linking of the PE layer and loose polymer chain packing.

Both TD-IP_β and TD-IP_γ membranes achieved much higher water permeance than the control PA and CD/MPD-TMC membranes, reaching values of 10.0 ± 3.1 and 8.4 ± 3.9 LMH•bar^{-1}, respectively. These values represent a more than 6-fold increase in water permeance as compared to the control PA membrane, and more than 3-fold increase as compared to the best performing CD/MPD-TMC membrane. TD-IP membranes are essentially PE (β/γ) membranes where the surface has been modified with MPD. TD-IP_β and TD-IP_γ membranes showed AO dye rejections of 98.5 % and 98.6 %, respectively. These rejection values are much higher than those observed for the PE_β and PE_γ (AO rejection <85 %). This suggests that the incorporation of MPD monomers acts as a "curing agent" and seals the defects of the PE sublayer. According to SEM and TEM analysis, TD-IP membranes present a porous structure where the selective layer is believed to be present in the vicinity of the pores, otherwise dye rejection above 98 % could not be achieved. Fig. 8 shows that this particular membrane structure is capable of achieving large water permeances, probably due to the high pore connectivity. It is hypothesized that the formation of a PE sublayer, which is loose and very permeable, acts as a "gutter layer" for the selective layer that is synthesized on top of the PE via inversed IP with unreacted TMC molecules and MPD molecules.

The MWCO of the membranes was examined using PEG solutions of 200, 400, 600 and 1500 Da (Fig. 9) to assess the membrane rejection of neutral molecules, and consequently, their molecular sieving capabilities. The pure PA TFC exhibits a MWCO of around 400 Da, which is consistent with a highly cross-linked PA layer having strong molecular sieving effects [37]. Both TD-IP_β and TD-IP_γ membranes show moderate rejection across all PEG solutions, including the highest molecular weight PEG of 1500 Da. This suggests that the size exclusion performance of the TD-IP membranes is reduced compared to that of the pure PA membrane suggesting poor sieving effects of the PE layer containing the CDs. Consequently, there are not significant differences between membranes containing the two types of CDs (β/γ).

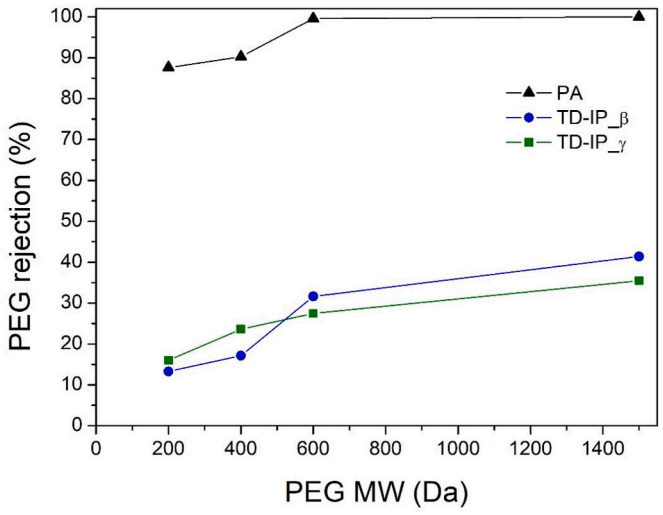

Fig. 9. MWCO of pure PA (triangles) and TD-IP_β (circles) and TD-IP_γ (squares) membranes using PEG solutions at 5 g l^{-1}.

TEM experiments of TD-IP membranes identify the presence of a dense polymer on top of the porous support, characteristic of NF membranes. These membranes are capable of rejecting low molecular weight compounds due to molecular sieving effects, dielectric repulsions, and the Donnan effect. MWCO studies (Fig. 9) indicate that TD-IP membranes exhibit modest rejection rates for neutral molecules. This suggests poor molecular sieving capabilities, and therefore the predominant AO rejection mechanisms are electrostatic repulsions and the Donnan effect. Such phenomena have been recognized as effective mechanisms for dye rejection in various NF membranes [38,39]. As depicted in Fig. 8, PE membrane demonstrates limited ability to reject AO dye (<85 % rejection), yet TD-IP membranes exhibit above 98 % rejection of the dye. Given that TD-IP is composed of a PE layer that has been further modified with MPD, it is evident that this surface modification plays a major role in the rejection performance. In PE membranes, positively charged AO dye are attracted to terminal carboxylic groups on the membrane surface. However, after MPD incorporation and forming TD-IP membranes, the membrane surface exhibit repulsive interactions,

both electrostatic and Donnan, between the terminal amines and positively charged AO molecules, hindering the passage of the dye through the membrane.

3.3. Comparison with literature

The use of CDs for NF applications has been widely reported, either as a substitute for the amine monomer to form pure PE layers or in combination with an amine monomer to fabricate PE/PA membranes.

CDs have been utilized to replace MPD monomers due to the porous and non-toxic nature of these macromolecules. Tesha et al. prepared tight ultrafiltration membranes, using β-CD and TMC as monomers, capable of rejecting up to 96 % of bovine serum albumin protein [16]. An impressive water permeance of 104 LMH•bar^{-1} and a rejection close to 100 % of relatively large organic molecules, such as Congo Red (Mw = 697 g•mol^{-1}), was achieved by Liu et al. when using 4 wt% of β-CD, 0.2 wt% of TMC and 0.5•mol L^{-1} of NaOH for the synthesis of PE TFC membranes [17]. Xue et al. reported IP reactions of β-CD and graphene oxide (GO) quantum dots with TMC resulting in TFCs capable of rejecting 93 % of Congo red with a water permeance of 474 LMH•bar^{-1} [40]. In another work, it was found that the preparation of PE membranes from β-CD and TMC led to steady water permeance and high dye rejections even after 96 h of chlorine exposure (10,000 ppm NaClO aqueous solution) [41]. The synthesis of PE TFCs from β-CD and TMC over modified multiwalled carbon nanotubes (MWCNT) substrates showed a pure water permeance of 180 LMH•bar^{-1} and a 96 % rejection of Congo red due to the presence of a porous network support layer [42].

In order to achieve high rejection rates for small organic molecules or inorganic divalent salts, the formation of PE/PA layers is frequently preferred over pure PE membranes. For instance, PIP and β-CD were added to the polyethersulfone (PES) dope solution employed to prepare the membrane support by phase inversion process. After the coagulation of the polymer and formation of an asymmetric PES membrane, PIP and β-CD remained on the pores of the PES membrane support and then reacted with TMC producing a PE/PA selective layer with a water permeance of 34 LMH•bar^{-1} and a 96 % rejection of Na_2SO_4 [15]. Malinga et al. reported poly (propyleneimine)-functionalized β-CD as a monomer for IP with TMC leading to membranes with a pure water permeance of 2.7 LMH•bar^{-1} and a 72 % rejection of humic acid [43]. Functionalization of β-CD has also been explored to exploit the intrinsic properties of CDs. High rejection of Na_2SO_4 (80–90 %) along with a water permeance of 2.8–4.4 LMH•bar^{-1} was found by Wu et al. when reacting triethanolamine and TMC in the presence of β-CD or sulfated β-CD under basic pH conditions [44]. In another work, β-CD was chemically grafted to the basal plane of GO nanoflakes and incorporated into the PA matrix formed by reaction between PIP and TMC [14]. The resulting membranes demonstrated an improved rejection (100 % for hydrocarbons, 89 % for divalent salts, and 74 % for monovalent salts) and 80 % increase in pure water permeance (~17 LMH•bar^{-1}) due to the increased hydrophilicity of the membranes containing the nanofillers. A similar study was carried out by Matshetshe et al. where (β-CD)-functionalized GO was used as nanofiller in PA membranes prepared through IP between MPD and TMC [13]. The resulting membrane exhibited a 25 % increase in water permeance, maintained salt rejection above 95 % and demonstrated a steady permeance over 144 h of operation due to the improved antifouling and antimicrobial properties of the membrane. Wang et al. functionalized β-CD with PIM-1, a member of the polymers of intrinsic microporosity (PIM) family. This improved the compatibility between the CD-based nanofiller and the PA matrix, which was made of PIP and TMC [45]. The addition of the hybrid (PIM-1)-(β-CD) nanofiller resulted in a 3-fold increase in water permeance (15.3 LMH bar^{-1}) along with a 95 % rejection of Na_2SO_4.

The utilization of γ-CD is relatively limited due to its large pore size, which is often considered to result in lower selectivity. γ-CD was combined with PIP and reacted with TMC, resulting in membranes with excellent rejection of antibiotics (>99 %) and high water permeance (26 LMH•bar^{-1}) [12]. In another study, Zhao et al. reported an enhancement in membrane hydrophilicity due to the addition of the γ-CD to PA. This led to an increase in water permeance (4.9 LMH•bar^{-1}) together with the induction of sieving effects from the γ-CD nanochannels that resulted in a Li/Mg selectivity of 10.8 [18].

The strategy presented in this manuscript, based on TD-IP process, has not previously been reported and offers several advantages over the aforementioned studies. This strategy maximizes the main features of CDs that make them attractive for NF applications, such as hydrophilicity and high porosity. This is achieved through the formation of a PE layer modified with MPD molecules on the surface. In this structure, the PE layer acts as a "gutter layer" owing to the intrinsic porosity of the CDs, while the top layer containing MPD molecules enables appropriate dye rejection. In addition, WCA revealed that TD-IP membranes show greater hydrophilicity than PA membranes due to the presence of several hydroxyl groups contained in both types of CDs. Our approach specifically focuses on the challenging task of rejection of low molecular weight dyes, such as AO. To achieve this, a PA layer was prepared using MPD and TMC monomers. This is known to be the preferred combination for producing tight NF membranes with excellent rejection performance. However, this approach can be modified, e.g. substituting MPD by PIP monomers, to achieve a more open structure, significantly increasing water permeance, when a less demanding rejection performance is required.

4. Conclusions

PA membranes combined with two types of CDs (β- and γ-) have been prepared and evaluated for water NF of AO orange dye (265 Da). Two strategies were followed to incorporate the CDs to the PA layers: i) formation of a blended PE/PA layer (CD/MPD-TMC membranes), and ii) a TD-IP method based on the formation of a PE layer followed by surface modification with MPD molecules. Both approaches led to higher water permeances as compared to control pure PA membranes, but the later exhibited a much larger increase in permeance while maintaining dye rejection at high standards (>98 %). Membrane characterization revealed that the incorporation of the CDs increases the hydrophilicity of the membrane selective layers, which contributes to the higher water permeances observed. TD-IP membranes displayed high water permeation (10 LMH•bar^{-1}) and excellent AO dye rejection (>98 %). The large increase in water permeance is related to the formation of a membrane consisting of a loose and very permeable PE layer, rich of hydrophilic hydroxyl groups from CDs, modified with MPD molecules. The incorporation of MPD onto the membrane surface accounts for the high AO dye rejection due to electrostatic and Donnan repulsions.

Credit author statement

Cristina Pina-Vidal: Conceptualization, Methodology, Formal analysis, Investigation, Visualization.

Jose Miguel Luque-Alled*: Conceptualization, Methodology, Investigation, Writing - Original Draft, Writing - Review & Editing, Supervision.

Joaquín Coronas: Conceptualization, Writing - Review & Editing, Funding acquisition.

Carlos Téllez*: Conceptualization, Methodology, Investigation, Writing - Review & Editing, Supervision, Funding acquisition.

Declaration of competing interest

The authors declare that they have no known competing financial interests or personal relationships that could have appeared to influence the work reported in this paper.

Data availability

No data was used for the research described in the article.

Acknowledgment

This research gratefully acknowledges grant PID2019-104009RB-I00 funded by MCIN/AEI/10.13039/501100011033 (Agencia Estatal de Investigación (AEI) and Ministerio de Ciencia e Innovación (MCIN), Spain). J. M. Luque-Alled acknowledges Grant FJC2021-047822-I funded by MCIN/AEI/10.13039/501100011033 and by the European Union NextGenerationEU/PRTR, and Margarita Salas funded by Ministerio de Universidades and by the European Union NextGenerationEU/PRTR. In addition, financial support from the Aragón Government (T43-20R, T68_23R). Authors acknowledge Servicio General de Apoyo a la Investigación-SAI and the use of instrumentation as well as the technical advice provided by the National Facility ELECMI ICTS, node Laboratorio de Microscopias Avanzadas (LMA), both at Universidad de Zaragoza.

Appendix A. Supplementary data

Supplementary data to this article can be found online at https://doi.org/10.1016/j.mtsust.2023.100593.

References

[1] Unknown, World Economic Forum, 2017.
[2] K.P. Lee, T.C. Arnot, D. Mattia, A review of reverse osmosis membrane materials for desalination—development to date and future potential, J. Membr. Sci. 370 (2011) 1–22, https://doi.org/10.1016/J.MEMSCI.2010.12.036.
[3] R.S. Harisha, K.M. Hosamani, R.S. Keri, S.K. Nataraj, T.M. Aminabhavi, Arsenic removal from drinking water using thin film composite nanofiltration membrane, Desalination 252 (2010) 75–80, https://doi.org/10.1016/J.DESAL.2009.10.022.
[4] M. Röhricht, J. Krisam, U. Weise, U.R. Kraus, R.A. Düring, Elimination of pharmaceuticals from wastewater by submerged nanofiltration plate modules, Desalination 250 (2010) 1025–1026, https://doi.org/10.1016/J.DESAL.2009.09.098.
[5] A. De Munari, A.J.C. Semiao, B. Antizar-Ladislao, Retention of pesticide Endosulfan by nanofiltration: influence of organic matter–pesticide complexation and solute–membrane interactions, Water Res. 47 (2013) 3484–3496, https://doi.org/10.1016/J.WATRES.2013.03.055.
[6] P.S. Zhong, N. Widjojo, T.S. Chung, M. Weber, C. Maletzko, Positively charged nanofiltration (NF) membranes via UV grafting on sulfonated polyphenylenesulfone (sPPSU) for effective removal of textile dyes from wastewater, J. Membr. Sci. 417 (2012) 52–60, https://doi.org/10.1016/J.MEMSCI.2012.06.013, 418.
[7] V. Berned-Samatán, C. Rubio, A. Galán-González, E. Muñoz, A.M. Benito, W. K. Maser, J. Coronas, C. Téllez, Single-walled carbon nanotube buckypaper as support for highly permeable double layer polyamide/zeolitic imidazolate framework in nanofiltration processes, J. Membr. Sci. 652 (2022), 120490, https://doi.org/10.1016/J.MEMSCI.2022.120490.
[8] S. Sorribas, P. Gorgojo, C. Téllez, J. Coronas, A.G. Livingston, High flux thin film nanocomposite membranes based on metal–organic frameworks for organic solvent nanofiltration, J. Am. Chem. Soc. 135 (2013) 15201–15208, https://doi.org/10.1021/ja407665w.
[9] X. Li, Y. Liu, J. Wang, J. Gascon, J. Li, B. Van der Bruggen, Metal–organic frameworks based membranes for liquid separation, Chem. Soc. Rev. 46 (2017) 7124–7144, https://doi.org/10.1039/C7CS00575J.
[10] L. Paseta, J.M. Luque-Alled, M. Malankowska, M. Navarro, P. Gorgojo, J. Coronas, C. Téllez, Functionalized graphene-based polyamide thin film nanocomposite membranes for organic solvent nanofiltration, Sep. Purif. Technol. 247 (2020), 116995, https://doi.org/10.1016/J.SEPPUR.2020.116995.
[11] S. Abdikheibari, W. Lei, L.F. Dumée, N. Milne, K. Baskaran, Thin film nanocomposite nanofiltration membranes from amine functionalized-boron nitride/polypiperazine amide with enhanced flux and fouling resistance, J. Mater. Chem. A 6 (2018) 12066–12081, https://doi.org/10.1039/C8TA03446J.
[12] T. Zhang, H. Zhang, P. Li, S. Ding, X. Wang, Highly permeable composite nanofiltration membrane via γ-cyclodextrin modulation for multiple applications, Sep. Purif. Technol. 297 (2022), 121541, https://doi.org/10.1016/J.SEPPUR.2022.121541.
[13] K. Matshetshe, K. Sikhwivhilu, G. Ndlovu, P. Tetyana, N. Moloto, Z. Tetana, Antifouling and antibacterial β-cyclodextrin decorated graphene oxide/polyamide thin-film nanocomposite reverse osmosis membranes for desalination applications, Sep. Purif. Technol. 278 (2021), 119594, https://doi.org/10.1016/J.SEPPUR.2021.119594.
[14] A.Q. Al-Gamal, T.A. Saleh, F.I. Alghunaimi, Nanofiltration membrane with high flux and oil rejection using graphene oxide/β-cyclodextrin for produced water reuse, Mater. Today Commun. 31 (2022), 103438, https://doi.org/10.1016/J.MTCOMM.2022.103438.
[15] Y. Liu, J. Zhu, J. Zheng, X. Gao, J. Wang, X. Wang, Y.F. Xie, X. Huang, B. Van der Bruggen, A facile and scalable fabrication procedure for thin-film composite membranes: integration of phase inversion and interfacial polymerization, Environ. Sci. Technol. 54 (2020) 1946–1954, https://doi.org/10.1021/acs.est.9b06426.
[16] J.M. Tesha, D.S. Dlamini, S. Qaseem, Z. Cui, J. Li, Tight ultrafiltration: layer deposition of Trimesoyl chloride/β-Cyclodextrin onto Polysulfone/Poly (styrene-co-maleic anhydride) membrane for water treatment, J. Environ. Chem. Eng. 8 (2020), 103733, https://doi.org/10.1016/J.JECE.2020.103733.
[17] L. Liu, L. Yu, B. Borjigin, Q. Liu, C. Zhao, D. Hou, Fabrication of thin-film composite nanofiltration membranes with improved performance using β-cyclodextrin as monomer for efficient separation of dye/salt mixtures, Appl. Surf. Sci. 539 (2021), 148284, https://doi.org/10.1016/J.APSUSC.2020.148284.
[18] Y. Zhao, N. Li, J. Shi, Y. Xia, B. Zhu, R. Shao, C. Min, Z. Xu, H. Deng, Extra-thin composite nanofiltration membranes tuned by γ-cyclodextrins containing amphipathic cavities for efficient separation of magnesium/lithium ions, Sep. Purif. Technol. 286 (2022), 120419, https://doi.org/10.1016/J.SEPPUR.2021.120419.
[19] A.I. Ramos, T.M. Braga, P. Silva, J.A. Fernandes, P. Ribeiro-Claro, M. de F.S. Lopes, F.A.A. Paz, S.S. Braga, Chloramphenicol·cyclodextrin inclusion compounds: co-dissolution and mechanochemical preparations and antibacterial action, CrystEngComm 15 (2013) 2822–2834, https://doi.org/10.1039/C3CE26414A.
[20] E. Patyk-Kaźmierczak, M.R. Warren, D.R. Allan, A. Katrusiak, Pressure inverse solubility and polymorphism of an edible γ-cyclodextrin-based metal–organic framework, Phys. Chem. Chem. Phys. 19 (2017) 9086–9091, https://doi.org/10.1039/C7CP00593H.
[21] L. Paseta, M. Navarro, J. Coronas, C. Téllez, Greener processes in the preparation of thin film nanocomposite membranes with diverse metal-organic frameworks for organic solvent nanofiltration, J. Ind. Eng. Chem. 77 (2019) 344–354, https://doi.org/10.1016/J.JIEC.2019.04.057.
[22] L. Paseta, D. Antorán, J. Coronas, C. Téllez, 110th anniversary: polyamide/metal–organic framework bilayered thin film composite membranes for the removal of pharmaceutical compounds from water, Ind. Eng. Chem. Res. 58 (2019) 4222–4230, https://doi.org/10.1021/acs.iecr.8b06017.
[23] H. Sun, S. Bao, H. Zhao, Y. Chen, Y. Wang, C. Jiang, P. Li, Q. Jason Niu, Polyarylate membrane with special circular microporous structure by interfacial polymerization for gas separation, Sep. Purif. Technol. 251 (2020), 117370, https://doi.org/10.1016/J.SEPPUR.2020.117370.
[24] C. Guo, N. Li, X. Qian, J. Shi, M. Jing, K. Teng, Z. Xu, Ultra-thin double Janus nanofiltration membrane for separation of Li+ and Mg2+: "Drag" effect from carboxyl-containing negative interlayer, Sep. Purif. Technol. 230 (2020), 115567, https://doi.org/10.1016/J.SEPPUR.2019.05.009.
[25] D.W. Mangindaan, N.M. Woon, G.M. Shi, T.S. Chung, P84 polyimide membranes modified by a tripodal amine for enhanced pervaporation dehydration of acetone, Chem. Eng. Sci. 122 (2015) 14–23, https://doi.org/10.1016/j.ces.2014.09.014.
[26] D.W. Mangindaan, G. Min Shi, T.-S. Chung, Pervaporation dehydration of acetone using P84 co-polyimide flat sheet membranes modified by vapor phase crosslinking, J. Membr. Sci. 458 (2014) 76–85, https://doi.org/10.1016/j.memsci.2014.01.030.
[27] F. Topuz, A.Y. Shaikh, M.O. Guler, T. Uyar, Water-insoluble polymer-free uniform nanofibers of peracetylated cyclodextrin by electrospinning, J. Mater. Sci. 55 (2020) 11752–11762, https://doi.org/10.1007/s10853-020-04820-2.
[28] A.B. Ganganboina, R. Doong, Functionalized N-doped graphene quantum dots for electrochemical determination of cholesterol through host-guest inclusion, Microchim. Acta 185 (2018) 526, https://doi.org/10.1007/s00604-018-3063-4.
[29] A. Akbari, Z. Derikvandi, S.M. Mojallali Rostami, Influence of chitosan coating on the separation performance, morphology and anti-fouling properties of the polyamide nanofiltration membranes, J. Ind. Eng. Chem. 28 (2015) 268–276, https://doi.org/10.1016/J.JIEC.2015.03.002.
[30] K. Fan, Y. Liu, X. Wang, P. Cheng, S. Xia, Comparison of polyamide, polyesteramide and polyester nanofiltration membranes: properties and separation performance, Sep. Purif. Technol. 297 (2022), 121579, https://doi.org/10.1016/j.seppur.2022.121579.
[31] W. Cai, M. Wang, G.Q. Yang, J. Li, High-performance nanofiltration membranes with a polyamide-polyester composite layer and a polydopamine surface layer for desalination and dye pollutant removal, Polymer 268 (2023), 125720, https://doi.org/10.1016/j.polymer.2023.125720.
[32] M.F. Jimenez Solomon, Y. Bhole, A.G. Livingston, High flux membranes for organic solvent nanofiltration (OSN)—interfacial polymerization with solvent activation, J. Membr. Sci. 423 (2012) 371–382, https://doi.org/10.1016/J.MEMSCI.2012.08.030, 424.
[33] X. Wu, M. Shaibani, S.J.D. Smith, K. Konstas, M.R. Hill, H. Wang, K. Zhang, Z. Xie, Microporous carbon from fullerene impregnated porous aromatic frameworks for improving the desalination performance of thin film composite forward osmosis membranes, J. Mater. Chem. A 6 (2018) 11327–11336, https://doi.org/10.1039/C8TA01200H.
[34] L. Paseta, C. Echaide-Górriz, C. Téllez, J. Coronas, Vapor phase interfacial polymerization: a method to synthesize thin film composite membranes without using organic solvents, Green Chem. 23 (2021) 2449–2456, https://doi.org/10.1039/D1GC00236H.
[35] B. Zhu, R. Shao, N. Li, C. Min, S. Liu, Z. Xu, X. Qian, L. Wang, Progress of cyclodextrin based-membranes in water treatment: special 3D bowl-like structure to achieve excellent separation, Chem. Eng. J. 449 (2022), 137013, https://doi.org/10.1016/j.cej.2022.137013.

[36] A. Cid-Samamed, J. Rakmai, J.C. Mejuto, J. Simal-Gandara, G. Astray, Cyclodextrins inclusion complex: preparation methods, analytical techniques and food industry applications, Food Chem. 384 (2022), 132467, https://doi.org/10.1016/J.FOODCHEM.2022.132467.

[37] J.M. Luque-Alled, L. Martínez-Izquierdo, P. Gorgojo, C. Téllez, J. Coronas, Organic solvent-free fabrication of thin film polyamide/zeolitic imidazolate framework membranes for removal of dyes from water, Chem. Eng. J. 470 (2023), 144233, https://doi.org/10.1016/J.CEJ.2023.144233.

[38] Y.F. Mi, N. Wang, Q. Qi, B. Yu, X.D. Peng, Z.H. Cao, A loose polyamide nanofiltration membrane prepared by polyether amine interfacial polymerization for dye desalination, Sep. Purif. Technol. 248 (2020), 117079, https://doi.org/10.1016/J.SEPPUR.2020.117079.

[39] T.T. Van Tran, S.R. Kumar, S.J. Lue, Separation mechanisms of binary dye mixtures using a PVDF ultrafiltration membrane: Donnan effect and intermolecular interaction, J. Membr. Sci. 575 (2019) 38–49, https://doi.org/10.1016/J.MEMSCI.2018.12.070.

[40] J. Xue, J. Shen, R. Zhang, F. Wang, S. Liang, X. You, Q. Yu, Y. Hao, Y. Su, Z. Jiang, High-flux nanofiltration membranes prepared with β-cyclodextrin and graphene quantum dots, J. Membr. Sci. 612 (2020), 118465, https://doi.org/10.1016/J.MEMSCI.2020.118465.

[41] J. Xue, Z. Jiao, R. Bi, R. Zhang, X. You, F. Wang, L. Zhou, Y. Su, Z. Jiang, Chlorine-resistant polyester thin film composite nanofiltration membranes prepared with β-cyclodextrin, J. Membr. Sci. 584 (2019) 282–289, https://doi.org/10.1016/J.MEMSCI.2019.04.077.

[42] J. Li, J.L. Gong, G.M. Zeng, B. Song, W.C. Cao, S.Y. Fang, S.Q. Tang, Y. Guan, Z. K. Tan, Z.P. Chen, X.Q. Mao, R.L. Zhu, Thin-film composite polyester nanofiltration membrane with high flux and efficient dye/salts separation fabricated from precise molecular sieving structure of β-cyclodextrin, Sep. Purif. Technol. 276 (2021), 119352, https://doi.org/10.1016/J.SEPPUR.2021.119352.

[43] S.P. Malinga, O.A. Arotiba, R.W.M. Krause, S.F. Mapolie, M.S. Diallo, B.B. Mamba, Cyclodextrin-dendrimer functionalized polysulfone membrane for the removal of humic acid in water, J. Appl. Polym. Sci. 130 (2013) 4428–4439, https://doi.org/10.1002/app.39728.

[44] H. Wu, B. Tang, P. Wu, Preparation and characterization of anti-fouling β-cyclodextrin/polyester thin film nanofiltration composite membrane, J. Membr. Sci. 428 (2013) 301–308, https://doi.org/10.1016/J.MEMSCI.2012.09.063.

[45] Z. Wang, S. Guo, B. Zhang, L. Zhu, Hydrophilic polymers of intrinsic microporosity as water transport nanochannels of highly permeable thin-film nanocomposite membranes used for antibiotic desalination, J. Membr. Sci. 592 (2019), 117375, https://doi.org/10.1016/J.MEMSCI.2019.117375.